Watching Carbon Nanotube Forest Growth using X-rays

Eric R. Meshot[1], Mostafa Bedewy[1], Sameh Tawfick[1], K. Anne Juggernauth[1], Eric Verploegen[2], Yongyi Zhang[1], Michael De Volder[1], and A. John Hart[1]

[1]*Department of Mechanical Engineering, University of Michigan*
[2]*Department of Materials Science and Engineering, MIT*

Carbon nanotubes (CNTs) have many potential applications due to their atomic structure and consequent mechanical[1], electrical[2] and thermal[3] properties. CNTs can be classified into two distinct structural forms: (i) a single seamless cylindrical shell of sp^2-bonded carbon atoms arranged in a honeycomb lattice constituting a single-wall CNT (SWCNT) which typically has a diameter ranging from 0.4 nm to 3nm; (ii) several concentric seamless shells with 0.34 nm inter-wall spacing, forming a multi-wall CNT (MWCNT) which can have diameters ranging from 1.4 nm to 100 nm. An infinitely long assembly of aligned, continuous, and densely packed CNTs would constitute the ultimate of synthetic fibers, and could have several times the strength of piano wires at one-fourth the density, along with thermal and electrical conductivity exceeding copper. However, before this dream is realized, many smaller-scale configurations of CNTs are potentially useful for next-generation transistors, flexible and transparent electronics, and multifunctional interface layers. Specifically, vertically aligned CNT "forests", consisting of tens of billions of CNTs per square centimeter on a flat substrate, are widely sought as high-performance electrical, thermal, and mechanical interface layers, as well as filtration membranes[4-10].

Although CNTs can be synthesized by many methods involving high-temperature decomposition and reorganization of solid carbon, the most popular and scalable means of CNT synthesis is catalytic chemical vapor deposition, where CNTs "grow" from metal catalyst nanoparticles that are typically placed on a substrate or floated in a carbon-containing gas atmosphere. The process of CNT forest growth by thermal CVD typically involves multiple stages: (1) the catalyst is prepared on a substrate, such as a silicon wafer; (2) the catalyst is heated and treated chemically, such as by exposure to a reducing atmosphere that causes agglomeration of a thin film into nanoparticles; (3) the catalyst is exposed to a carbon-containing atmosphere, which causes formation and "liftoff" of CNTs from the nanoparticles on the substrate; and (4) CNT growth continues by competing pathways between accumulation of "good" (graphitic) and "bad" (amorphous) carbon[11]. To engineer the functional properties of CNT materials such as forests, we must develop reaction processes that not only treat these stages independently, but that are also accompanied by characterization techniques that enable mapping of the forest characteristics for large sample sizes and populations. Despite extensive study of aligned CNT forest production[12-27], including recent advances using water and oxygen as additives to increase reaction yield and catalyst lifetime, the limiting mechanisms of forest growth are not fully understood, and CNT forest heights are typically limited to several millimeters. In Figure 1, we show an AFM image of nanoparticles arranged for CNT forest growth, as well as images of a vertically aligned multi-wall CNT forest at different magnifications.

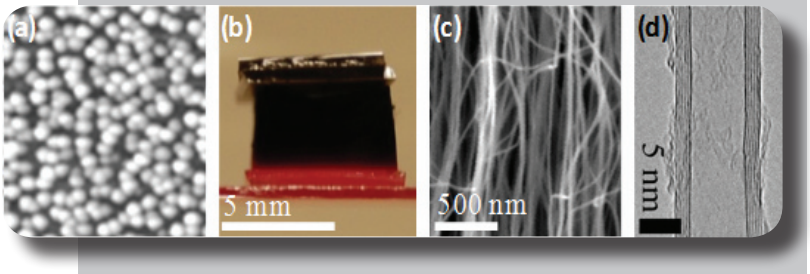

Fig. 1: (a) 500 nm AFM scan of Fe nanoparticles formed on an Al_2O_3 support layer by heating in H_2 for 2 minutes at 825 °C; and vertically aligned multi-wall CNTs at different magnifications: (b) 10 X, (c) 140,000 X (SEM) and (d) 7,000,000 X (TEM).

At CHESS, we use *ex situ* and *in situ* small-angle X-ray scattering (SAXS) to investigate growth of CNT forests, and work closely with Dr. Arthur Woll, Prof. Sol Gruner, and colleagues. In order to elucidate the dynamics of catalyst particle coarsening, forest self-organization, temperature- and reactant-driven CNT structure evolution, and growth termination in realtime, a custom-built atmospheric-pressure CVD reactor featuring a resistively heated substrate platform[28], shown in Figure 2, is mounted directly in the G1 beamline at CHESS, enabling *in situ* grazing incidence (GI-SAXS) and transmission (SAXS, WAXS) scattering studies, as shown in Figure 3. Simultaneous laser measurement of the forest height captures the growth kinetics, the heated platform enables rapid temperature changes (200 °C/s) during annealing and growth, and the reactant gas is independently heated to create a population of active carbon species that cause efficient CNT growth. Further, Figure 3 summarizes the different techniques and resulting data for both GI and transmission modes: we show schematics of our setups, examples of scattering intensities collected by the FLICAM detector, and data demonstrating temperature effects on nanoparticle and CNT formation.

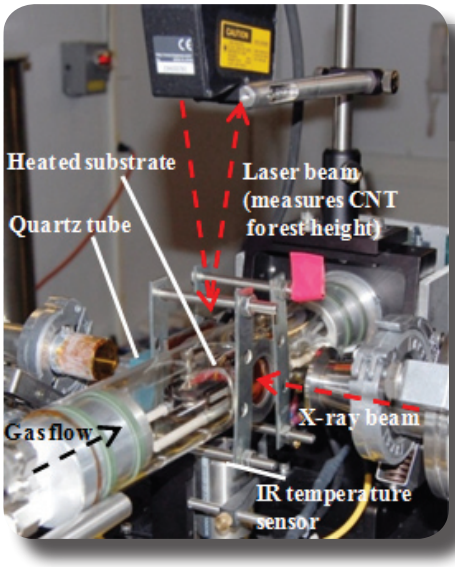

Fig. 2: Photograph of CNT growth apparatus mounted in the G1 Beamline.

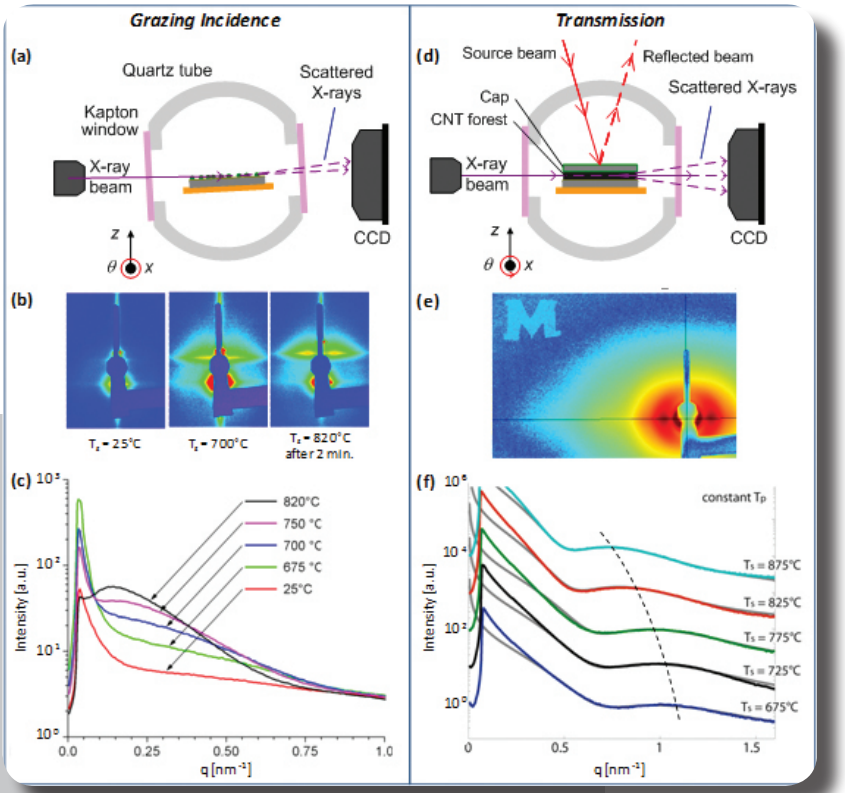

Fig. 3: Schematic and data for both grazing incidence (a-c) and transmission (d-f) SAXS configurations. For GI mode: (a) schematic shows X-rays glancing off substrate-bound particles; (b) scattering intensity from a population of Fe nanoparticles forming in real time as temperature increases; (c) *I* vs. *q* profiles showing real-time evolution of the structure factor peak for the Fe nanoparticles. For transmission mode: (d) schematic shows X-rays passed directly through a CNT forest; (e) representative scattering intensity from a CNT forest; (f) *I* vs. *q* profiles with curve fits showing the dependence of the CNT form factor peak on growth temperature – the shift of the peak position to lower *q* indicates larger CNT mean diameter.

After growth, we also carry out *ex situ* characterization of the CNT forests in order to spatially map their bulk morphology[29]. Using SAXS we can investigate the spatial variations in MWCNT orientation. In addition we use SAXS to measure a locally averaged spatial variation in CNT diameters within our films. CNT diameters obtained by fitting the scattering results were confirmed by TEM imaging, which establishes SAXS as an attractive non-destructive technique for precisely examining CNT materials[29,30].

Starting with a catalyst thin-film of Fe/Al_2O_3 on Si, we observe rapid coarsening of Fe at temperatures as low as 650 °C (Figure 3c)[31]. CNT diameter and growth rate are directly proportional to the substrate temperature (Figure 3f)[30], and tuning of annealing and growth conditions using SAXS-derived diameter measurements reveals that CNT forests with mean diameters ranging from 4-20 nm can be grown from the same starting catalyst film thickness (not shown here)[31]. Growth self-terminates abruptly, accompanied by a sudden loss of alignment at the CNT-substrate interface (Figure 4); this appears to be a universal chemical and/or mechanical signature in our experiments[32]. Our apparatus and investigative technique offer significant potential to further understand the limiting mechanisms of CNT forest growth, and for rapid tuning of process conditions to engineer application-oriented structural characteristics of nanotubes and nanowires.

Figure 4a shows *in situ* measurements of the height evolution of a forest that self-terminates, and of forests which are terminated prematurely by rapidly cooling the substrate or stopping the flow of the carbon containing gas while maintaining the substrate temperature[33]. As seen in Figure 4b, the orientation (quantified by the Hermans orientation parameter) increases sharply at the top of a forest, representing the transition from tangled to vertically aligned morphology during the first stage of growth. The orientation then remains approximately constant as growth proceeds, and then it decays steeply toward zero before growth terminates, indicating the onset of disordered CNTs. In agreement with the morphological evolution indicated by the calculated Hermans values, SEM images (Figure 4c) show that the self-terminated forest exhibits disorder at its base, yet the intentionally terminated forests exhibit strong alignment at the base. This demonstrates that the loss of alignment is a signature of growth self-termination, and is not caused by cooling the reactor or by an abrupt decrease in the carbon concentration in the CVD atmosphere.

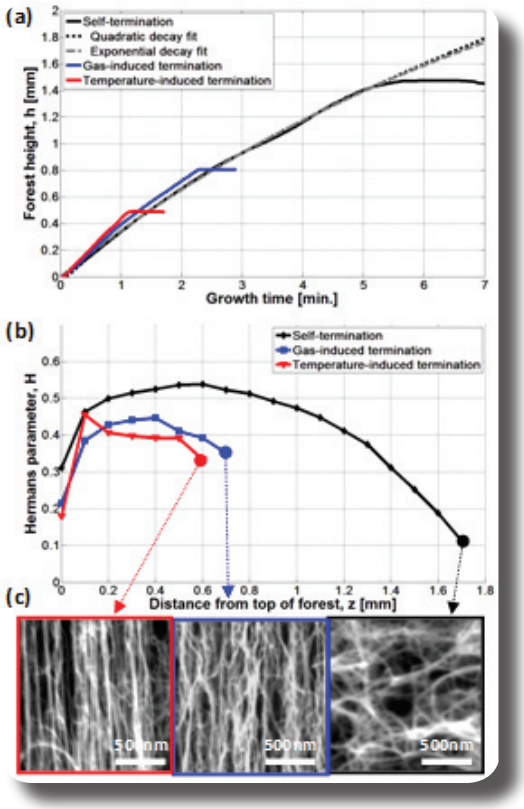

Fig. 4: (a) Growth kinetics for 3 CNT forests for different growth times under otherwise identical conditions are plotted along with theoretical quadratic and exponential decay curves. (b) Relative alignment within each forest is quantified, and (c) corresponding SEM images verify the CNT morphology.

Based on our *in situ* and *ex situ* results, we explain the evolution and termination of CNT forest growth based on a collective model consisting of four stages[33], as illustrated in Figure 5:

I. nucleation and self-assembly of randomly oriented CNTs into a vertically aligned forest structure;
II. steady growth, wherein the number density of growing CNTs remains constant with time;
III. density decay, wherein the number density of CNTs within the forest decreases with time; and
IV. abrupt termination, wherein forest growth ceases suddenly, and is accompanied by a loss of CNT alignment at the interface between the CNTs and the substrate.

In conclusion, we have employed nondestructive X-ray techniques for rapid characterization of CNT forests, revealing dynamics of their growth and termination processes and enhancing our ability to better engineer the characteristics of these forests (i.e., length, density, CNT diameter). Further, we have developed *in situ* GI methods with our custom CVD apparatus for probing the dynamics of catalyst particle formation from thin films for CVD of CNTs. By observing the agglomeration and coarsening of these particles in real time, we elucidate this rapid process as we move toward understanding the different chemical states and transitions of the particles as well as the prerequisites for stabilizing populations of small particles for small-diameter CNT growth. These applied techniques may also be adapted for comprehensive studies of other systems of 1-dimensional (nanotubes, nanowires) and 0-dimensional (nanoparticles) structures, demonstrating the impact and versatility of such characterization methods for understanding how to create new materials and nanostructures.

The Mechanosynthesis Group's X-ray team (Figure 6) makes the following acknowledgements. This work was funded by the University of Michigan Department of Mechanical Engineering and College of Engineering, and the National Science Foundation (CMMI-0800213). E. R. Meshot and S. Tawfick are grateful for University of Michigan Mechanical Engineering Departmental Fellowships. E. A. Verploegen is grateful to the Institute for Soldier Nanotechnologies at MIT, funded by the U.S. Army Research Office (DAAD-19-02-D0002). Some studies (Figure 3f) based from methods developed at CHESS were conducted at the National Synchrotron Light Source, Brookhaven National Laboratory, which is supported by the U.S. Department of Energy Office of Basic Energy Sciences (DE-AC02-98CH10886). Otherwise, X-ray scattering was performed at CHESS, which is supported by the National Science Foundation and the National Institutes of Health under Grant No. DMR-0225180. SEM and TEM were performed at the University of Michigan Electron Microbeam Analysis Laboratory (EMAL). We thank Jong G. Ok, Sangwoo Han, Myounggu Park, Arthur Woll, Mark Tate, Hugh Philipp, Marianne Hromalik, and Sol Gruner for assistance with X-ray scattering experiments and analysis.

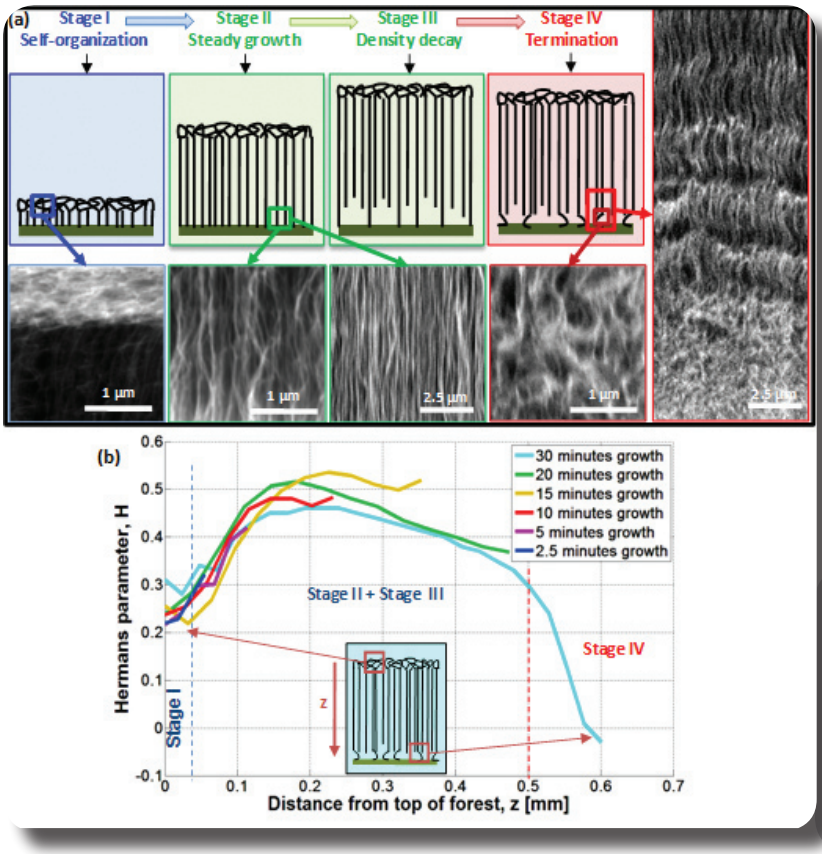

Fig. 5: Collective growth mechanism of a CNT forest: (a) growth stages; and SEM images of the tangled crust at top of forest, aligned morphology at bottom during steady growth, and the randomly oriented morphology at bottom, induced by density decay and abrupt self-termination; (b) time evolution of Hermans orientation parameter for forests grown for different durations in a "hot wall" tube furnace..

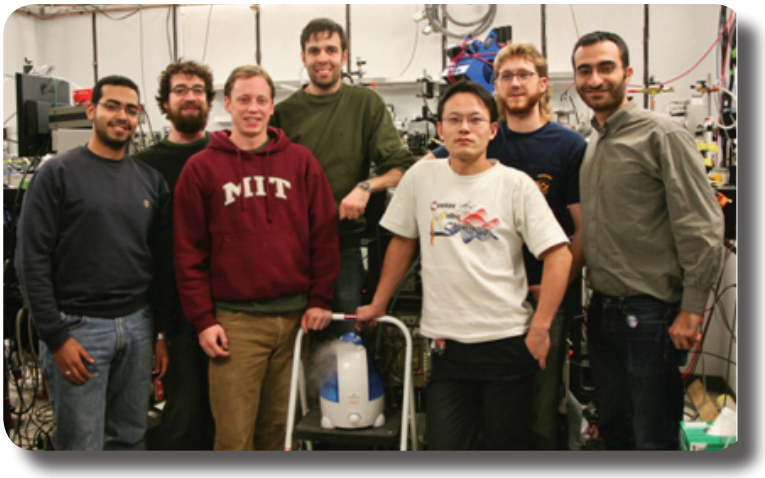

Fig. 6: Mechanosynthesis Group's X-ray team in the hutch at G1 line.

From left to right: Mostafa Bedewy, Michael de Volder, Eric Verploegen, John Hart, Penguin, Yongyi Zhang, Eric Meshot, and Sameh Tawfick.

References:

1. N. Yao, and V. Lordi; Journal of Applied Physics 1998, 84 (**4**), 1939-1943 (1998)
2. H.J. Li, W.G. Lu, J.J. Li, X.D. Bai, and C.Z. Gu; Physical Review Letters, 95 (**8**), 086601 (2005)
3. P. Kim, L. Shi, A. Majumdar, and P.L. McEuen; Physical Review Letters, 87 (**21**), 215502 (2001)
4. R.H. Baughman, A.A. Zakhidov, and W.A. de Heer; Science, 297 (**5582**), 787-792 (2002)
5. M. Endo, T. Hayashi, Y. Kim, M. Terrones, and M. Dresselhaus; Philosophical Transactions of the Royal Society of London Series A-Mathematical Physical and Engineering Sciences, 362 (**1823**), 2223-2238 (2004)
6. E.J. Garcia, B.L. Wardle, and A.J. Hart; Composites Part a-Applied Science and Manufacturing, 39 (**6**), 1065-1070 (2008)
7. T. Tong, Y. Zhao, L. Delzeit, A. Kashani, M. Meyyappan, and A. Majumdar; Transactions on Components and Packaging Technologies, 30 (**1**), 92-100 (2007)
8. W. Choi, D. Chung, J. Kang, H. Kim, Y. Jin, I. Han, Y. Lee, J. Jung, N. Lee, G. Park, and J. Kim; Applied Physics Letters, 75 (**20**), 3129-3131(1999)
9. J. Holt, H. Park, Y. Wang, M. Stadermann, A. Artyukhin, C. Grigoropoulos, A. Noy, and O. Bakajin, Science, 312 (**5776**), 1034-1037 (2006)
10. B. Hinds, N. Chopra, T. Rantell, R. Andrews, V. Gavalas, and L. Bachas; Science, 303 (**5654**), 62-65 (2004)
11. A.I. Lacava, C.A. Bernardo, and D.L. Trimm, Carbon, 20 (**3**), 219-223 (1982)
12. L. Dell'Acqua-Bellavitis, J. Ballard, P. Ajayan, and R. Siegel; Nano Letters, 4 (**9**), 1613-1620 (2004)
13. E. Einarsson, Y. Murakami, M. Kadowaki, and S. Maruyama; Carbon, 46 (**6**), 923-930 (2008)
14. D. Futaba, K. Hata, T. Yamada, K. Mizuno, M. Yumura, and S. Iijima; Physical Review Letters, 95 (**5**) (2005)
15. J. Han, R. Graff, B. Welch, C. Marsh, R. Franks, and M. Strano; ACS Nano, 2 (**1**), 53-60 (2008)
16. K. Liu, K. Jiang, C. Feng, Z. Chen, and S. Fan; Carbon, 43 (**14**), 2850-2856 (2005)
17. O. Louchev, T. Laude, Y. Sato, and H. Kanda; Journal of Chemical Physics; 118 (**16**), 7622-7634 (2003)
18. A. Puretzky, D. Geohegan, S. Jesse, I. Ivanov, and G. Eres; Applied Physics A-Materials Science & Processing, 81 (**2**), 223-240 (2005)
19. R. Xiang, Z. Yang, Q. Zhang, G. Luo, W. Qian, F. Wei, M. Kadowaki, E. Einarsson, and S. Maruyama; Journal of Physical Chemistry C, 112 (**13**), 4892-4896 (2008)
20. L. Zhu, J. Xu, F. Xiao, H. Jiang, D. Hess, and C. Wong; Carbon, 45 (**2**), 344-348 (2007)
21. L. Zhu, D. Hess, and C. Wong; Journal of Physical Chemistry B, 110 (**11**), 5445-5449 (2006)
22. G.Y. Zhang, D. Mann, L. Zhang, A. Javey, Y.M. Li, E. Yenilmez, Q. Wang, J.P. McVittie, Y. Nishi, J. Gibbons, and H.J. Dai; Proceedings of the National Academy of Sciences of the United States of America, 102 (**45**), 16141-16145 (2005)
23. K. Hata, D.N. Futaba, K. Mizuno, T. Namai, M. Yumura, S. Iijima; Science, 306 (**5700**), 1362-1364 (2004)
24. S.S. Fan, M.G. Chapline, N.R. Franklin, T.W. Tombler, A.M. Cassell, and H.J. Dai; Science, 283 (**5401**), 512-514 (1999)
25. L. Delzeit, C.V. Nguyen, B. Chen, R. Stevens, A. Cassell, J. Han, and M. Meyyappan; Journal of Physical Chemistry B, 106 (**22**), 5629-5635 (2002)
26. A. Hart, and A. Slocum; Journal of Physical Chemistry, 110 (**16**), 8250-8257 (2006)
27. R.F. Wood, S. Pannala, J.C. Wells, A.A. Puretzky, and D.B. Geohegan; Physical Review B, 75 (**23**), 8 (2007)
28. L. van Laake, A.J. Hart, and H.H. Slocum; Review of Scientific Instruments, 78 (**8**) (2007)
29. B.N. Wang, R.D. Bennett, E. Verploegen, A.J. Hart, and R.E. Cohen; Journal of Physical Chemistry C, 111 (**16**), 5859-5865 (2007)
30. E.R. Meshot, D.L. Plata, S. Tawfick, E.A. Verploegen, and A.J. Hart; (Submitted 2009)
31. A.J. Hart, E. Verploegen, and E.R. Meshot; (In preparation 2009)
32. E. Meshot, and A. Hart; Applied Physics Letters, 92 (**11**) (2008)
33. M. Bedewy, E.R. Meshot, H. Guo, E.A. Verploegen W. Lu, and A.J. Hart; (Submitted 2009)